PROCEEDINGS OF SCIENCE

Ion acceleration in 3D hybrid simulations of non-relativistic quasi-perpendicular shocks

Luca Orusa[a,b,*] **and Damiano Caprioli**[c,d]

[a] *Department of Physics, University of Torino, via P. Giuria, 1, 10125 Torino, Italy*

[b] *Istituto Nazionale di Fisica Nucleare, via P. Giuria, 1, 10125 Torino, Italy*

[c] *Department of Astronomy & Astrophysics, University of Chicago, Chicago, IL 60637, USA*

[d] *Enrico Fermi Institute, The University of Chicago, Chicago, IL 60637, USA*

E-mail: luca.orusa@edu.unito.it

Understanding the conditions conducive to particle acceleration at collisionless, non-relativistic shocks is important for the origin of cosmic rays. We use hybrid (kinetic ions—fluid electrons) kinetic simulations to investigate particle acceleration and magnetic field amplification at non-relativistic, weakly magnetized, quasi-perpendicular shocks. So far, no self-consistent kinetic simulation has reported non-thermal tails at quasi-perpendicular shocks. Unlike 2D simulations, 3D runs show that protons develop a non-thermal tail spontaneously (i.e., from the thermal bath and without pre-existing magnetic turbulence). They are rapidly accelerated via shock drift acceleration up to a maximum energy determined by their escape upstream. We discuss the implications of our results for the phenomenology of heliospheric shocks, supernova remnants and radio supernovae. For further information about this work refer to [1].

38th International Cosmic Ray Conference (ICRC2023)
26 July - 3 August, 2023
Nagoya, Japan

*Speaker

PoS(ICRC2023)263

1. Introduction

Understanding the conditions that promote particle acceleration at collisionless, non-relativistic shocks is crucial for comprehending the origin of cosmic rays and for the phenomenology of heliospheric shocks, novae, supernova remnants (SNRs), winds and lobes of active galaxies, and galaxy clusters. The main process responsible for energization at shocks is diffusive shock acceleration (DSA) [2], where particles are scattered back and forth across the shock discontinuity, gaining energy through a series of first-order Fermi cycles. To fully account for the non-linear interplay between particle acceleration and self-generated magnetic turbulence at non-relativistic shocks, numerical kinetic simulations are essential. Full particle-in-cells (PIC) simulations have successfully captured ion and electron DSA at quasi-parallel shocks (where the angle between the background field $\mathbf{B}_0$ and the shock normal is $\vartheta_{\rm Bn} \lesssim 45^\circ$) [3]. However, evidence of DSA at (quasi-)perpendicular shocks ($\vartheta_{\rm Bn} \approx 90^\circ$) has been elusive in simulations performed in 1D [4], 2D [5], and 3D [6]. Full-PIC simulations can cover only a restricted range of time/space scales. To address more macroscopic systems, hybrid simulations with kinetic ions and fluid electrons have played a pivotal role in advancing our understanding of ion DSA at non-relativistic shocks. Previous 2D simulations have shown that thermal ions can be *spontaneously* injected into DSA at quasi-parallel shocks [7–9], while the injection of ions at oblique and quasi-perpendicular shocks has been more problematic. While test-particle and Monte Carlo calculations with prescribed strong scattering seem to support ion injection [10], no self-consistent kinetic simulation has reported DSA tails. Nevertheless, hybrid simulations *augmented* with upstream magnetic fluctuations with long-wavelength and large amplitudes [11] suggest that quasi-perpendicular shocks may be efficient ion accelerators. If the magnetic turbulence is artificially seeded by hand in the pre-shock medium [10], or when energetic seeds are added [12], DSA may occur for arbitrary inclinations. However, the efficiency and spectra of DSA in such scenarios are not universal and depend critically on the *ad-hoc* prescriptions for the pre-existing seeds and turbulence. The absence of non-thermal tails in 1D/2D simulations is likely due to the artificial suppression of particle diffusion across field lines [10, 13]. A significant question remains regarding whether 3D cross-field diffusion of supra-thermal particles can lead to *spontaneous* injection into DSA. To address this, we employ hybrid simulations to explore quasi-perpendicular shocks across the magnetized to weakly-magnetized regime. The results demonstrate that even for non-relativistic shocks, ion acceleration occurs naturally if the ordered magnetic field is sufficiently low and the full 3D dynamics are retained. For further information about this work refer to [1].

2. Simulation setup

Simulations are performed with the `dHybrid` non-relativistic code [14]. We send a supersonic flow with speed $v_{\rm sh}$ against a reflecting wall (left boundary), which produces a shock moving right into a quasi-perpendicular $\mathbf{B}_0$ field with $\vartheta_{\rm Bn} = 80^\circ$. Lengths are measured in units of the ion skin depth $d_i \equiv c/\omega_p$, where c is the light speed and $\omega_p \equiv \sqrt{4\pi n e^2/m}$ is the ion plasma frequency, with m, e and n the ion mass, charge and number density, respectively. Time is measured in inverse cyclotron times $\omega_c^{-1} \equiv mc/(eB_0)$. Velocities are normalized to the Alfvén speed $v_A \equiv B/\sqrt{4\pi mn}$ and energies to $E_{\rm sh} \equiv m v_{\rm sh}^2/2$. Simulations include the three spatial components of the particle

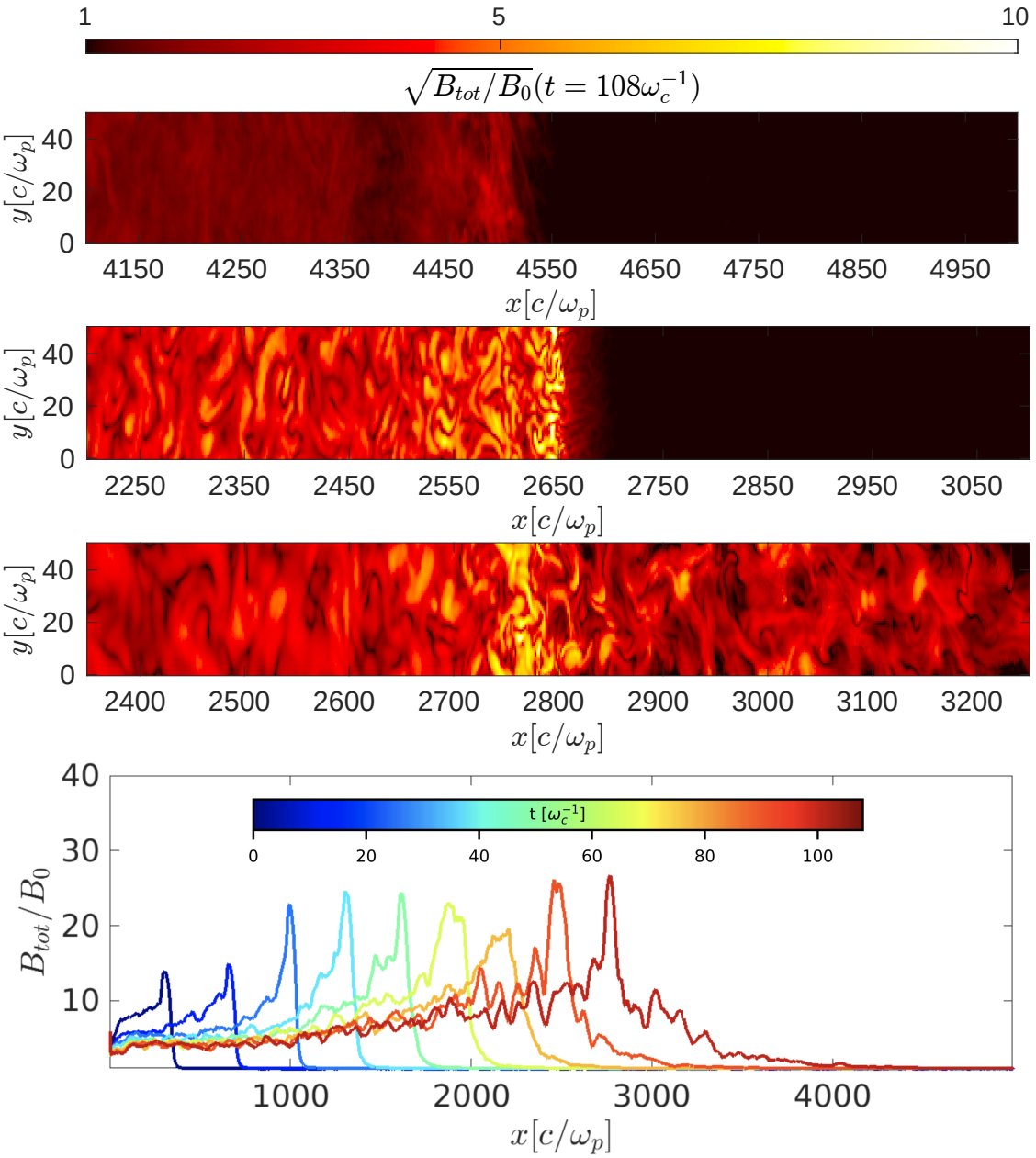

Figure 1: From the top: Total magnetic field for the out-of-plane (2Dz), in-plane (2Dy), and 3D setups. Bottom panel: evolution of $B_{\rm tot}$ in 3D. In all cases M=100 and $t = 108\omega_c^{-1}$.

momentum and of the electromagnetic fields. Ions are initialized with thermal velocity $v_{\rm th} = v_A$ and electrons are an adiabatic fluid initially in thermal equilibrium. We define the sonic Mach number as $M_{\rm s} \equiv v_{\rm sh}/c_{\rm s}$, with $c_{\rm s}$ the speed of sound and the Alfvénic Mach number as $M_A \equiv v_{\rm sh}/v_A$; throughout the paper we indicate the shock strength simply with $M = M_A \simeq M_s$. We performed simulations with different M, longitudinal sizes, and time steps, as reported on the left side of Table I of Ref. [1]; the transverse sizes are fixed to $50d_i$ in all the cases. We use two and a half cells

per d_i in each direction and 8 (4) ion particles per cell in 3D (2D).

3. Results

We start our analysis by comparing the dynamics of quasi-perpendicular shocks in various dimensions: 1D, 2D with **B** lying either in the plane (referred to as 2Dy) or out of the plane (referred to as 2Dz), and 3D.

Amplification of Magnetic Field. The total intensity of the magnetic field $B_{\rm tot}$ is presented in Fig. 1 for a shock with $M = 100$ and $\vartheta_{\rm Bn} = 80°$ in 2Dz, 2Dy, and a slice in the $x - y$ plane of the 3D configurations. The lower panel shows the evolution of $B_{\rm tot}$ in the 3D scenario. A noteworthy distinction is observed between 2Dz and 2Dy: in the former, the field is merely compressed at the shock, while in the latter, $B_{\rm tot}$ experiences overshooting and substantial amplification downstream [5]. In 3D, field amplification extends both upstream and downstream of the shock, a signature of the existence of a precursor generated by back-streaming particles. The divergence between 2Dz and 2Dy is attributed to the presence of a finite baroclinic term, which is limited to the z component in 2D. This suggests a contribution of turbulent dynamo processes as well.

Particle Spectra and Dependence on M. The upper panel of Fig. 2 displays the post-shock ion spectrum at $t = 108\omega_c^{-1}$ for distinct setups: while 1D and 2D manifest only a supra-thermal bump [7], 3D exhibits an extended power-law tail. The dashed line represents a Maxwellian distribution with a temperature approximately 80% of the one of a purely gaseous shock. It's notable that the post-shock magnetic turbulence in 2Dy, although quite similar to the 3D scenario, is insufficient to inject particles into the acceleration process. The middle panel of Fig. 2 shows the evolution of the downstream ion spectrum in 3D: from an initial supra-thermal bump, a non-thermal tail emerges, spanning over three orders of magnitude in about $100\omega_c^{-1}$. The bottom panel of Fig. 2 shows the spectra for different Mach numbers. Each spectrum is a power-law, $f(E) \propto E^{-\alpha}$, characterized by an acceleration efficiency ε, representing the fraction of post-shock energy density contained in ions with energy exceeding $10E_{\rm sh}$. For $M = 100$, the spectrum tends towards $E^{-1.5}$ ($\propto p^{-4}$ for non-relativistic particles), the profile expected in strong shocks. For lower M values, the non-thermal tails become steeper and less extended, almost vanishing for $M = 20$. The post-shock magnetic turbulence scales as $\propto \sqrt{M}$, which increases the probability of ions to jump upstream, leading to harder spectra. Overall, the acceleration efficiency scales from a few percent for $M = 20$ to $\varepsilon \gtrsim 20\%$ for $M \gtrsim 50$, a level analogous to the efficiency of quasi-parallel shocks [7].

Acceleration mechanism. Fig. 3 (left panel) illustrates the trajectory in the $x - p_x$ plane and the energy gain of an ion tracked for $M = 30$. The energy gain occurs through shock drift acceleration (SDA), where particles tap into the motional electric fields during their gyrations around the shock [15]. Cross-field diffusion, as emphasized in [10, 13], significantly contributes to the ions' return from downstream and is fully captured only in 3D. [13] demonstrated that charged particles in an arbitrary electromagnetic field with at least one ignorable spatial coordinate remain forever tied to a B-field line. Since in 2D the field lines are effectively transverse "sheets", ion diffusion along the shock normal is suppressed. In contrast, in 3D, field lines can twist, intertwine, and allow cross-field diffusion of ions, effectively preventing them from being rapidly swept downstream.

Constraints on Maximum Achievable Energy? Fig. 3 (right panel) shows the time evolution of the maximum ion energy $E_{\rm max}$ for varying M. Following an initial growth $\propto t^2$, $E_{\rm max}$ consistently

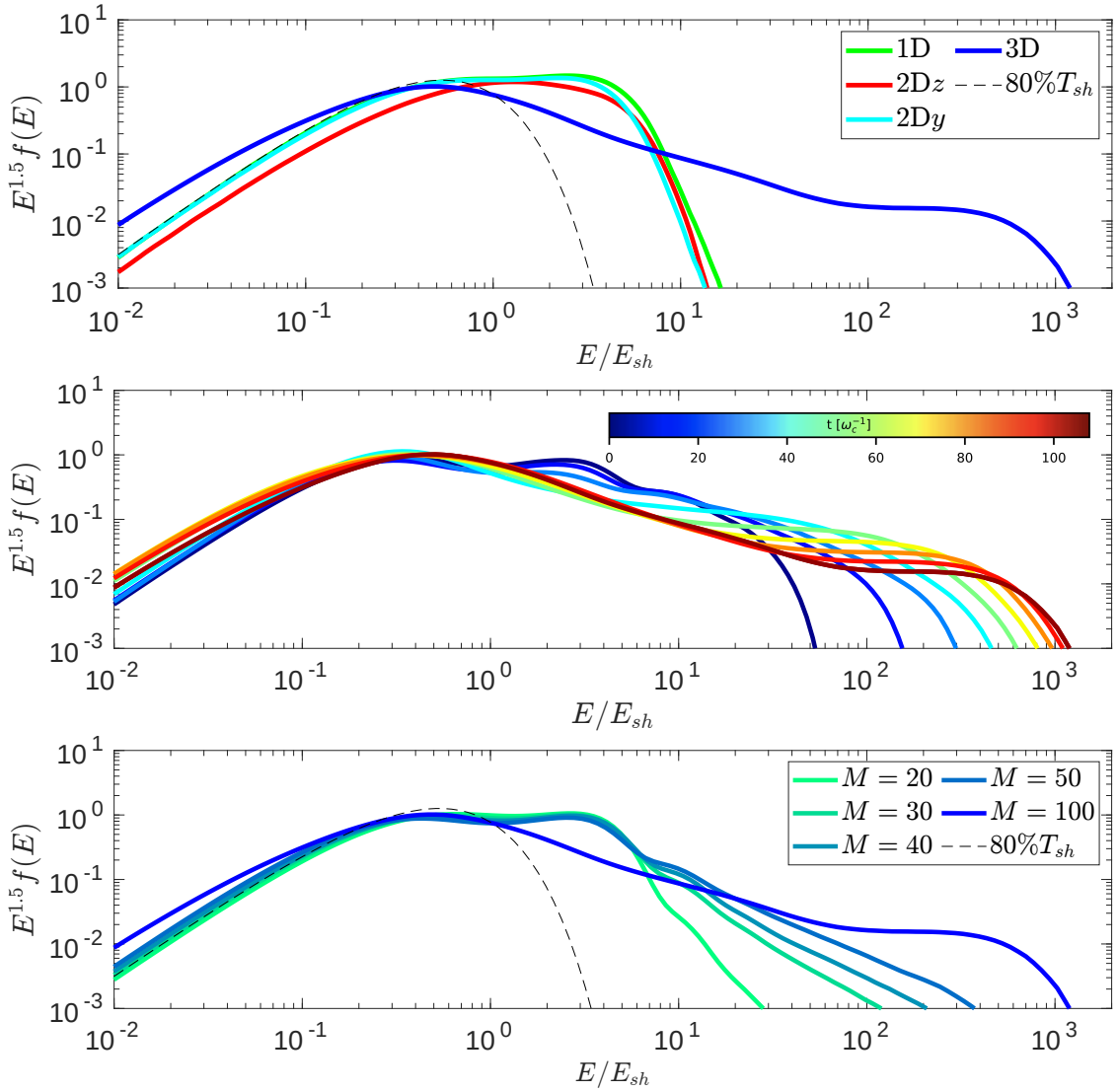

Figure 2: Top panel: downstream ion spectrum at $t = 108\omega_c^{-1}$ for $M = 100$ and different setups. Middle panel: time evolution of the ion spectrum in 3D. Bottom panel: spectrum dependence on M; the dashed line indicates a Maxwellian with temperature $\sim 80\%$ of the one expected for a purely gaseous shock.

levels off at an asymptotic value $E^*_{\rm max}$, scaling $\propto M$ due to the larger number of SDA cycles ions can undergo. For non-relativistic ions, the momentum gain per SDA cycle is $\Delta p/p \propto v_{\rm sh}/v$, where v is the ion speed, implying a constant $\Delta p \propto v_{\rm sh}$. Since each SDA cycle lasts roughly $\Delta t \approx \omega_c^{-1}$ (independent of v), and given that the cycle count $\propto t$, then $p_{\rm max} \propto \Delta p t/\omega_c^{-1} \rightarrow E_{\rm max} \propto t^2$. For relativistic particles, $\Delta p \propto p$ and $\Delta t \propto \omega_c^{-1} p$, leading to $E_{\rm max} \propto t$. This acceleration process is remarkably fast with respect to DSA even for relativistic ions, as DSA's cycle duration is the diffusion time $\sim p/v_{\rm sh}\omega_c^{-1}$. At later stages and for higher M values, there is a brief shift from SDA to DSA. Some sufficiently energetic ions return to the shock via pitch-angle diffusion rather than ordered gyration (producing the deviation from the $\propto t^2$ curve before the plateau in the right panel

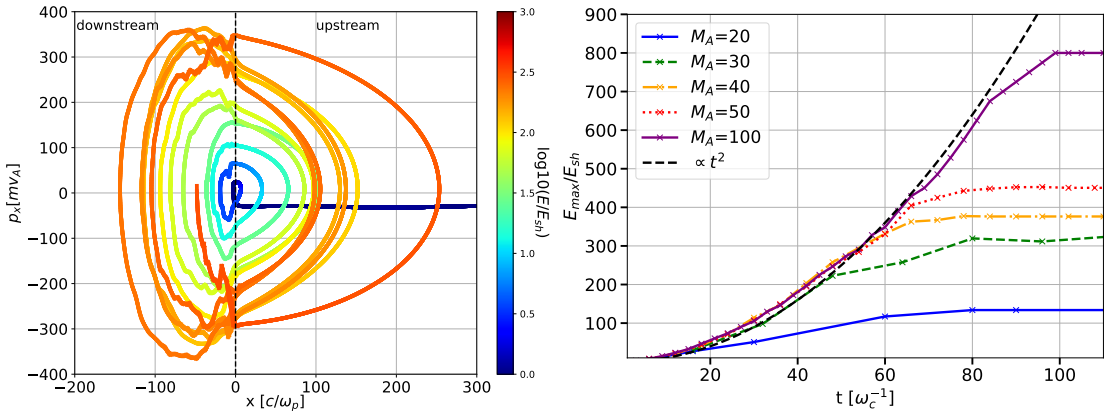

Figure 3: Left panel: energy gain (color code) and trajectory in the $x - p_x$ plane of a representative ion undergoing SDA for M_A=30. Right panel: evolution of $E_{\max}(t)$ for different M; after an initial increase $\propto t^2$ provided by SDA (black solid line), $E_{\max}(t)$ eventually reaches an asymptotic value $\propto M$.

of Fig. 3). Eventually, ions escape towards upstream infinity, and the non-thermal tails stabilize at a critical energy $E^*_{\max} \propto M$. Whether the streaming of escaping ions could trigger the Bell instability [16] and thereby sustain self-driven acceleration to higher energies at later times is a problem that still has to be solved (see [17] for further information).

4. Phenomenological implications

The results described in this work have several applications in space/astrophysical shocks.

Heliospheric shocks. MMS measurements conducted at the Earth's bow shock reveal that quasi-parallel regions are more efficient in ion acceleration than oblique areas, as reported by [18]. Nonetheless, efficiencies of approximately $\varepsilon \lesssim 10\%$ for $\vartheta_{\rm Bn} \gtrsim 70^\circ$ align with our run at $M = 20$ but not with the outcomes from 2D simulations, which yield $\varepsilon \lesssim 1\%$ [7]. Another potential implication of the rapid acceleration we observe is in generating relativistic electrons within foreshock disturbances at the Earth's bow shock, as proposed by [19].

Supernova remnants. Of particular interest is the case of SN1006, which exhibits a bilateral symmetry determined by the orientation of $\mathbf{B}_0$ [20]. X/γ-ray emissions originate from the quasi-parallel (polar caps) zones, indicating the presence of multi-TeV electrons. In contrast, radio emissions display azimuthal symmetry [20], implying the existence of GeV electrons even in oblique regions. While effective ion DSA reaching multi-TeV energies aligns with the low polarization and intense synchrotron emissions in the polar caps, the acceleration of electrons in quasi-perpendicular regions is likely initiated through SDA, as discussed here. Subsequently, this acceleration could extend up to GeV energies due to interstellar turbulence [21]. Whether multi-TeV electrons should also be expected in quasi-perpendicular regions is an interesting question that hinges on the longer-term evolution of these systems [17].

Radio SNe. Radio emissions originating from young extragalactic SNe indicate that electrons are frequently accelerated with a spectral index $\alpha \simeq 3$ [22]. These steep spectra at high-speed shocks ($v_{\rm sh} \approx 10^4$ km s^{-1}) are challenging to reconcile with conventional diffusive shock acceleration (DSA), but they could align with the findings discussed here, given that $M \lesssim 50$. A supernova shock

propagating within the Parker spiral of the progenitor's wind may offer both relatively low Alfvénic Mach numbers and quasi-perpendicular shock geometries [22]. Scaling the asymptotic $E^*_{\rm max}$ as shown in Fig. 3 (right panel) by $v_{\rm sh} \simeq 10^4$ km s^{-1} for $M = 50$ yields $E^*_{\rm max} \simeq 0.22$GeV, suggesting that radio-emitting particles can be generated rapidly ($100\omega_c^{-1} \lesssim$ one minute for $B_0 \gtrsim 3$mG).

5. Conclusions

We used hybrid simulations to characterize —for the first time in kinetic calculations without any *ad-hoc* prescription for particle scattering and/or injection— how ions can be very rapidly accelerated at non-relativistic, quasi-perpendicular shocks. 3D simulations are necessary to fully capture the amplification of the initial magnetic field (Fig. 1) and the cross-field diffusion that allows ions not to be advected away downstream after a few shock crossings. Acceleration starts via SDA, exhibiting a clear signature $E_{\rm max} \propto t^2$, then briefly transitions to DSA (where $E_{\rm max} \propto t$) before reaching a limit energy $E^*_{\rm max}$, beyond which particles escape upstream. The spectral slope strongly depend on the shock Mach number M (see Fig. 2); also the level of magnetic field amplification and the maximum energy limit increase with M. We have briefly outlined few applications of our results to space/astrophysical shocks. The biggest questions that remain open are whether oblique/quasi-perpendicular shocks can efficiently drive plasma instabilities strong enough to self-sustain DSA up to energies significantly larger than $E^*_{\rm max}$, and whether the same acceleration process is viable for electrons, too.

References

[1] L. Orusa and D. Caprioli, *Fast particle acceleration in 3D hybrid simulations of quasi-perpendicular shocks*, *PRL, in press* (2023) [arXiv:2305.1051].

[2] A. R. Bell, *The acceleration of cosmic rays in shock fronts. I*, *MNRAS* **182** (Jan., 1978) 147–156.

[3] J. Park, D. Caprioli, and A. Spitkovsky, *Simultaneous Acceleration of Protons and Electrons at Nonrelativistic Quasiparallel Collisionless Shocks*, *Physical Review Letters* **114** (Feb., 2015) 085003, [arXiv:1412.0672].

[4] N. Shimada and M. Hoshino, *Strong electron acceleration at high mach number shock waves: Simulation study of electron dynamics*, *The Astrophysical Journal* **543** (nov, 2000) L67.

[5] A. Bohdan, M. Pohl, J. Niemiec, P. J. Morris, Y. Matsumoto, T. Amano, M. Hoshino, and A. Sulaiman, *Magnetic field amplification by the weibel instability at planetary and astrophysical shocks with high mach number*, *Phys. Rev. Lett.* **126** (Mar, 2021) 095101.

[6] Y. Matsumoto, T. Amano, T. N. Kato, and M. Hoshino, *Electron surfing and drift accelerations in a weibel-dominated high-mach-number shock*, *Physical Review Letters* **119** (sep, 2017).

[7] D. Caprioli and A. Spitkovsky, *Simulations of Ion Acceleration at Non-relativistic Shocks: I. Acceleration Efficiency*, *ApJ* **783** (Mar., 2014) 91, [arXiv:1310.2943].

[8] D. Caprioli and A. Spitkovsky, *Simulations of Ion Acceleration at Non-relativistic Shocks: II. Magnetic Field Amplification*, *ApJ* **794** (Oct., 2014) 46, [arXiv:1401.7679].

[9] D. Caprioli, A. Pop, and A. Spitkovsky, *Simulations and Theory of Ion Injection at Non-relativistic Collisionless Shocks*, *ApJL* **798** (Jan., 2015) 28, [arXiv:1409.8291].

[10] J. Giacalone and D. C. Ellison, *Three-dimensional numerical simulations of particle injection and acceleration at quasi-perpendicular shocks*, *JGR* **105** (June, 2000) 12541–12556.

[11] J. Giacalone, *The efficient acceleration of thermal protons by perpendicular shocks*, *ApJL* **628** (July, 2005) L37–L40.

[12] D. Caprioli, H. Zhang, and A. Spitkovsky, *Diffusive shock re-acceleration*, *JPP* (Jan., 2018) [arXiv:1801.0151].

[13] F. C. Jones, J. R. Jokipii, and M. G. Baring, *Charged-Particle Motion in Electromagnetic Fields Having at Least One Ignorable Spatial Coordinate*, *ApJ* **509** (Dec., 1998) 238–243, [astro-ph/9808103].

[14] L. Gargaté, R. Bingham, R. A. Fonseca, and L. O. Silva, *dHybrid: A massively parallel code for hybrid simulations of space plasmas*, *Computer Physics Communications* **176** (Mar., 2007) 419–425, [physics/0611174].

[15] G. Chen and T. P. Armstrong, *Acceleration of charged particles in oblique MHD shocks*, in *International Cosmic Ray Conference*, vol. 5 of *International Cosmic Ray Conference*, pp. 1814–1819, Aug., 1975.

[16] A. R. Bell, *Turbulent amplification of magnetic field and diffusive shock acceleration of cosmic rays*, *MNRAS* **353** (Sept., 2004) 550–558.

[17] E. R. Simon, D. Caprioli, C. Haggerty, and B. Reville, *Maximum energy achievable in supernova remnants: self-consistent simulations*, *PoS* **ICRC2023** (2023) 150.

[18] A. Lalti, Y. V. Khotyaintsev, A. P. Dimmock, A. Johlander, D. B. Graham, and V. Olshevsky, *A database of mms bow shock crossings compiled using machine learning*, *Journal of Geophysical Research: Space Physics* **127** (2022), no. 8 e2022JA030454.

[19] L. B. Wilson III, D. G. Sibeck, D. L. Turner, A. Osmane, D. Caprioli, and V. Angelopoulos, *Relativistic electrons produced by foreshock disturbances observed upstream of the Earth's bow shock*, *Phys. Rev. Lett.* **117** (Nov., 2016) 215101. Editors' Suggestion.

[20] R. Rothenflug, J. Ballet, G. Dubner, E. Giacani, A. Decourchelle, and P. Ferrando, *Geometry of the non-thermal emission in SN 1006. Azimuthal variations of cosmic-ray acceleration*, *A&A* **425** (Oct., 2004) 121–131.

[21] P. Blasi, *The origin of galactic cosmic rays*, *A&ARv* **21** (Nov., 2013) 70, [arXiv:1311.7346].

[22] R. A. Chevalier and C. Fransson, *Circumstellar emission from type ib and ic supernovae*, *ApJ* **651** (Nov., 2006) 381–391, [astro-ph/0607196].